ANNUAL REVIEWS

Annual Review of Physical Chemistry

Accelerated Reaction Kinetics in Microdroplets: Overview and Recent Developments

Zhenwei Wei,[1] Yangjie Li,[1] R. Graham Cooks,[1] and Xin Yan[2]

[1]Department of Chemistry, Purdue University, West Lafayette, Indiana 47907, USA; email: cooks@purdue.edu

[2]Department of Chemistry, Texas A&M University, College Station, Texas 77842, USA; email: xyan@tamu.edu

Annu. Rev. Phys. Chem. 2020. 71:31–51

The *Annual Review of Physical Chemistry* is online at physchem.annualreviews.org

https://doi.org/10.1146/annurev-physchem-121319-110654

Keywords

reaction acceleration, interfacial reactions, ion solvation, electrospray ionization, mass spectrometry

Abstract

Various organic reactions, including important synthetic reactions involving C–C, C–N, and C–O bond formation as well as reactions of biomolecules, are accelerated when the reagents are present in sprayed or levitated microdroplets or in thin films. The reaction rates increase by orders of magnitude with decreasing droplet size or film thickness. The effect is associated with reactions at the solution–air interface. A key factor is partial solvation of the reagents at the interface, which reduces the critical energy for reaction. This phenomenon is of intrinsic interest and potentially of practical value as a simple, rapid method of performing small-scale synthesis.

1. INTRODUCTION: BACKGROUND AND HISTORY

Mass spectrometry (MS), the art of ionization of compounds and manipulation of the resulting ions in vacuum, is widely used to measure the mass-to-charge ratios (*m/z*) of ionized compounds for their chemical characterization (1). However, besides its use as an analytical tool, one can also take advantage of the dilute gas phase of MS to perform chemical reactions. Since the 1970s, many organic ion/molecule reactions have been examined in the dilute gas phase of MS (2–5). Brauman and his coworkers (6–9) determined the rate constants of ion/molecule reactions and proposed the double-well energy surface to describe the effects of strong ion/molecule attractive forces in the absence of solvation. The results showed that ion/molecule reaction rates are often six orders of magnitude faster than the reaction rates in solution (2, 4, 10–12). This raises the question: Can one use MS as a synthetic tool based on this very high reactivity? Even today, this grand vision remains unfulfilled because of the low ion currents available for ionized molecules (13). However, MS has been used successfully as a synthetic tool: Back in the 1940s, as part of the Manhattan Project, calutron mass spectrometers were used to purify ^{235}U by *m/z* selection in sufficient amounts to construct the first nuclear weapon (14). Later, the development of ion soft-landing techniques enabled the purification and collection of organic molecules, including peptides, nucleotides, and proteins as gaseous ions with retention of some native bioactivity (15–20).

To further advance this idea, a key challenge is how the high reactivity and chemical specificity inherent in molecular ions generated by MS can be used to perform synthesis, ideally on a large scale and under ambient conditions. The introduction of electrospray ionization (ESI) by Fenn and colleagues (21) provides ready access to charged microdroplets under ambient conditions. Charged microdroplets can be considered a bridge between gas-phase (isolated) ions and those in reacting solutions. In 2006, the Eberlin transacetalization reaction (22), a well-studied ion/molecule reaction (23) occurring in dilute gas-phase conditions in MS, was studied by electrospraying charged microdroplets of tetramethylurea and directing them into a vapor of the neutral acetal. The yield of the Eberlin reaction product under ambient conditions was modest, but this experiment was among the first to indicate the likelihood of extremely high rate constants in microdroplet reactions.

The 2006 work encouraged a series of reactive desorption electrospray ionization (DESI) studies (24–26), many initially aimed at improving ionization efficiency by online chemical derivatization of compounds of analytical interest. Typically, the analyte was present on a solid surface and was examined using a spray of solvent containing the derivatizing reagent. In 2011, examination of the reaction between a ketone (ketosteroid) and hydrazine (Girard T reagent) to form the hydrazone using reactive DESI clearly showed reaction acceleration in microdroplets in air compared to the corresponding reaction in the bulk phase (27). Since then, the focus of this type of study has been divided between an interest in the mechanism of reaction acceleration in microdroplets and the applications of this phenomenon in organic synthesis. To accelerate reactions, investigators have developed a variety of microdroplet formats. These include preparative electrospray (28), thin-film deposition (29–36), microdroplets in sprays (37–45), the fusion of microdroplets (46, 47), various levitated droplet experiments (48–50), and multiphase microdroplet reactions (51). For the mechanistic studies, the lifetime and size of the microdroplets (52–54), the reagent distribution and orientation in the microdroplets (55, 56), mathematical models (34, 36, 56, 57), and computational chemistry (58) have been valuable in better understanding microdroplet physics and chemistry. Recently, the scope of accelerated chemistry in microdroplets has been extended (59, 60) to include catalyzed organic reactions and biomolecule transformations (61). Impetus for these studies is provided by the fact that reactions in small volumes might be relevant to unraveling biological processes in both cells and organelles as well as within membranes.

In this review, the term microdroplet refers to droplet diameters of less than 1,000 μm. We focus on four aspects of accelerated reaction kinetics in such droplets: (*a*) methodologies for performing microdroplet reactions, (*b*) the scope of microdroplet reaction chemistry, (*c*) mechanisms of microdroplet reaction acceleration, and (*d*) applications of accelerated microdroplet chemistry. We first review emerging technologies used to generate microdroplets and to perform reactions. We then compare the successful accelerated microdroplet reactions and summarize them based on their reaction types. We also attempt to combine the latest mechanistic findings to elucidate the mechanism of reaction acceleration in microdroplets. Lastly, we discuss several successful applications of accelerated microdroplet chemistry.

2. METHODOLOGY OF MICRODROPLET REACTIONS

In this section, we discuss how microdroplets have been generated and used as reaction vessels. The microdroplet reaction methodologies used so far are categorized into five types: (*a*) reactions in sprays, (*b*) reactions occurring during microdroplet collisions, (*c*) reactions occurring when microdroplets splash onto surfaces, (*d*) reactions in individual levitated microdroplets, and (*e*) reactions in thin films (**Figure 1**). Note that we do not consider systems with only liquid–liquid interfaces, where acceleration appears to be much more modest.

2.1. Reaction in Sprays

This section covers reactions occurring in confined individual microdroplets within an aerosol. Each microdroplet in the ensemble typically contains the reagents and catalysts for the reaction.

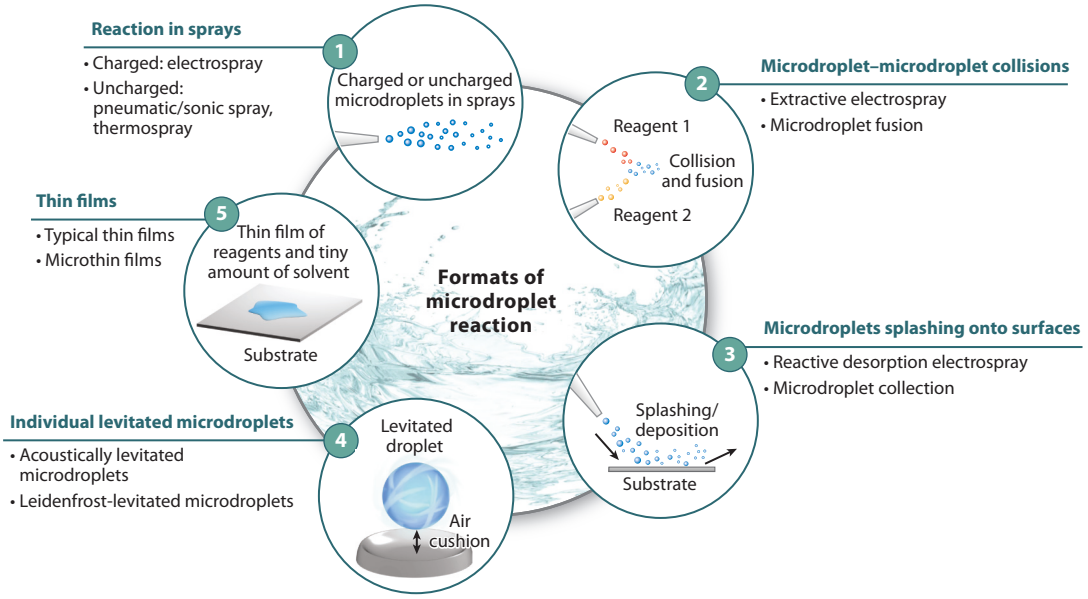

Figure 1

Five typical formats of microdroplet reactions. (❶) Reactions occur in charged or uncharged microdroplets generated by electrospray, pneumatic spray, etc. Each microdroplet contains the reagents and catalysts for the reaction. (❷) Reactions occur when two streams of microdroplets with different reagents meet, collide, and merge in a mixing region. (❸) Reactions occur when a stream of microdroplets is splashed onto a surface. This process has two modes: Microdroplets of reagents collide with a clean surface, or reagent in the microdroplets reacts with another reagent on the surface. (❹) Reactions occur in individual microdroplets levitated by acoustic, electromagnetic, or Leidenfrost levitation. (❺) Reactions occur when the reaction mixture forms a thin film on a substrate.

DIFFERENCE BETWEEN REACTION ACCELERATION AND REACTION MONITORING

Electrospray ionization mass spectrometry (ESI-MS) is a powerful tool that has been used in reaction monitoring for decades (65–67). When reaction monitoring is performed by continuous ESI-MS (68), DESI (69, 70), or nanoelectrospray ionization (nESI) (52, 71), reaction intermediates can be captured even when they have microsecond lifetimes, making it a valuable tool in the study of reaction mechanisms. However, care needs to be taken to distinguish between accelerating and nonaccelerating conditions under which microdroplets are examined. In reaction monitoring experiments, the sprayer/emitter is placed very close to the MS inlet to avoid reaction acceleration, thus ensuring nonaccelerating conditions. To study reaction acceleration, the sprayer/emitter is placed further from the MS inlet. The longer distance ensures a longer microdroplet lifetime and, with the appropriate solvent, allows evaporation and hence significant reaction acceleration in the smaller droplets.

Such microdroplets are usually generated in polydispersed form by spray methods under ambient conditions, e.g., electrospray (21), nanoelectrospray, sonic spray, or thermospray (62, 63). These microdroplet-generation methods were initially developed for analytical use as MS ionization sources. Although microdroplet acceleration experiments use the same equipment that is used in reaction monitoring, e.g., microdroplet generation followed by MS analysis, one needs to carefully distinguish between the two phenomena (see the sidebar titled Difference Between Reaction Acceleration and Reaction Monitoring). Another important point is that droplet size and lifetime affect the reaction rate, so one can observe quite different extents of reaction when varying the distance from the sprayer to the MS inlet. For example, the major product of Hantzsch synthesis of 1,4-dihydropyridines increased in relative intensity from less than 1% to becoming the dominant MS peak as the distance between the sprayer and inlet was increased from 20 cm to 90 cm (37). This is due to shrinkage of the droplet with solvent evaporation. A similar correlation between distance and conversion ratio ([product]/[reagent] or [P]/[R]) was observed for hydrazone formation from indoline-2,3-dione and phenyl hydrazine, the conversion ratio increasing from 40% to 90% as the distance increased from 1 cm to 8 cm (40). One needs to be careful in comparing reaction progress using the change-in-signal ratio of the product and reactant to represent the change-of-concentration ratio, as molecules in the same ESI droplet can have different ionization efficiencies and also can be formed by different ionization processes, causing ion loss to different extents when one changes distance or concentration (64). However, simple control experiments using mixtures of isolated reactant and product can be used to correct for these effects.

Zare and others (38, 39, 46, 47) have suggested that reactions in microdroplets are quenched when they enter the mass spectrometer through rapid desolvation. Therefore, the reaction time of the microdroplet is on the microsecond to millisecond scale, which was simply estimated by the distance divided by the microdroplet jet velocity. Mortensen & Williams (52) estimated microdroplet lifetimes in theta-emitter nESI experiments from knowledge of the kinetics of reduction of 2,6-dichloroindophenol by L-ascorbic acid, a reaction with a rate constant of 5.6×10^4 L mol^{-1} s^{-1}. In most microdroplet reaction experiments, variables such as droplet size, temperature, and concentration are not easy to hold constant, but one can make rough comparisons to bulk reactions and so obtain apparent acceleration factors (see the sidebar titled Definition of Apparent Acceleration Factors). The apparent acceleration factors can be very large in individual microdroplets, varying from 10^4 to 10^6 for the Claisen-Schmidt reaction, the Hantzsch reaction, and

DEFINITION OF APPARENT ACCELERATION FACTORS

Apparent acceleration factors are used to roughly compare reaction rates under different conditions, typically droplet versus bulk reactions. There are two ways to calculate an apparent acceleration factor. The first is to measure the time taken for the reactions in the two media to achieve the same conversion ratio. The other way is to let the reactions run for the same time and compare the conversion ratios. Many studies use the second method because it is easier to measure. The ratio of product concentration over reagent concentration ([P]/[R]) is usually defined as the conversion ratio; this value gives a linear relationship versus reaction time for a second-order reaction where the slope is the product of the rate constant and the initial reaction concentration.

the Pomeranz-Fritsch reaction (72). However, the loss of reagents and products in the open air and the limited reaction time of this format restrict the quantity of products that can be produced.

2.2. Microdroplet–Microdroplet Collisions

A reaction involving microdroplet–microdroplet collisions uses two streams of microdroplets, often as aerosols, to study accelerated reactions. When the two streams meet in the mixing region, microdroplet collisions may form a fused microdroplet or release smaller microdroplets through splashing. This method was first exploited for native MS analysis, namely as a form of extractive ESI, in which a stream of charged solvent microdroplets collides with another stream containing the biological sample and produces ionized biological molecules in the mixing region (73). Later, a similar technique was used for microdroplet reaction kinetics studies (46, 47, 74). The microdroplets in the two streams can be charged or uncharged and may be generated by ESI or pneumatic spray. The time from mixing to MS analysis is again in the microsecond to millisecond range. The apparent acceleration factor reported for this format is $\sim 10^3$ in the few cases studied (46, 47).

The microdroplet-collision format is particularly suitable for performing multiphase reactions (51). Many liquid–liquid heterogeneous reactions need phase-transfer catalysts for effective transport of reagent molecules between phases. In the microdroplet–microdroplet collision reaction format, microdroplets of immiscible solvents collide with each other; the forced mixing and fusion of microdroplets increase the interfacial area between the different phases and hence increase mass transfer (74). The oxidation of alcohols to aldehydes and ketones was reported to reach more than 50% yield on the millisecond timescale in this reaction format, avoiding use of phase-transfer catalysts. The angle between the two streams and the distance from the mixing region to the sprayers strongly influence the reaction yield by affecting the microdroplet-collision energy.

2.3. Microdroplets Splashing onto Surfaces

A typical microdroplet-splashing experiment is that known as reactive DESI (25, 27). In DESI, electrospray of solvent is used to desorb and ionize the analyte from a surface for subsequent MS analysis (75). The concept of reactive DESI is that a microdroplet stream containing a derivatizing reagent collides and reacts with the analyte on a substrate, leading to the release of the derivatized form of the analyte, which is then observed by MS. The reaction between Girard T reagent and ketosteroids to form hydrazone was found to show an apparent acceleration factor of 10^1 (27). When microdroplets collide with the substrate, the primary droplet (2.5–5 μm) forms secondary droplets (0.9–1.9 μm), which fall back to the substrate to form ring-shaped, thin films on the millisecond timescale. Accelerated reaction in the secondary droplets is evident from the increased concentration and surface-area-to-volume ratio. An alternative route to derivatization

is to deposit microdroplets of analyte mixed with derivatizing reagent on a substrate and then collect the product. In preparative ESI (28, 76), reaction acceleration can be achieved by collecting electrosprayed microdroplets on glass wool. One can also deposit neutral microdroplets continuously by pneumatic spray onto a variety of collecting substrates, e.g., polytetrafluoroethylene, paper, fiber, or metal, to achieve reaction acceleration (34). The emerging methods of preparative ESI and continuous microdroplet deposition have shown apparent acceleration factors of 10^2 to 10^4 (adjusted using reported values of [P]/([P]+[R]) at constant time) (28, 34). The results are independent of the choice of substrate material, indicating that the surface is not involved in the mechanism. This collection format supports demands for increased reaction scale, as one can easily adjust the flow rate of the sprayer. The largest scale so far reported is 120 mg h^{-1} for one sprayer (34). Obviously, one can achieve a larger scale easily by multiplexing.

2.4. Individual Levitated Microdroplets

This format focuses on the behavior and reactions in an individual microdroplet. Compared to microdroplets in an aerosol, levitated microdroplet techniques isolate an individual droplet, the volume of which varies from the nanoliter to microliter scale. Acoustic (ultrasonic) levitation is a good method to generate and manipulate individual microdroplets under ambient conditions (49). Beauchamp and colleagues (77) proposed the use of focused acoustic pulses to generate microdroplets for the study of interfacial reactions as well as to act as an ionization source for MS. Volmer and coworkers (49) found that acid-catalyzed erythromycin A degradation was accelerated by a factor of 10 in acoustically levitated microdroplets (~6 μL) compared to its rate of reaction in bulk conditions. Besides acoustic levitation, electric fields can also be applied to study individual microdroplet reactions. Recently, Wilson and coworkers (78) developed branched quadrupole traps to investigate imine formation when microdroplets merge in the trap.

Another droplet-levitation method implements the Leidenfrost effect. This physical phenomenon occurs when a liquid is close to a hot surface that is significantly hotter than the liquid's boiling point, producing a vapor cushion that levitates the liquid droplet (48). Leidenfrost droplet chemistry shows apparent acceleration factors in the range 10^1 to 10^2 (48, 50). The acceleration factor varies with the chemistry and the droplet size. The forced degradation reactions of active pharmaceutical ingredients such as tetracycline, trifluoperazine, and hydrochlorothiazide can be accelerated approximately 20 to 200 times, reducing the test time in forced stress workflows (50). Under Leidenfrost conditions, the evaporation of solvent is inevitable. For more precise reaction kinetics studies, a constant-volume, Leidenfrost-levitated droplet reaction format was developed by continuously adding solvent back into the droplet to compensate for solvent loss. With the solvent-addition capability, long-lived levitated droplets allow accelerated reactions to be run for long periods of time with the reaction acceleration separated from the analysis step. This format provides a way to determine reaction kinetics in microdroplets more precisely because of control over reaction concentration, time, and temperature.

2.5. Thin Films

Thin films share common features with microdroplets, and their reactions show similarities to the microdroplet chemistry we have been discussing. Features that both thin films and microdroplets share are the high surface-area-to-volume ratios and the degree of reagent confinement. The difference is that thin films may have interfaces with multiple phases, e.g., immiscible hydrophobic and hydrophilic solvents and precipitated solids after solvent evaporation, while the microdroplets discussed here are usually homogeneous. In a typical thin-film experiment, the reaction mixture is dropcast onto a substrate and the system is interrogated for the formation of products as a function

of the time after partial or full solvent evaporation (29–33). As solvent evaporates, new phases form, making thin films very complex reaction systems. Note that thin films also form when one collects microdroplets falling onto a substrate (27, 34). An advantage of thin films is their sometimes-long lifetime. For example, adding 10 pL of nonvolatile amine 3-(dimethylamino)-1-propylamine to a mixture of reagents in 500 nL of water gives a microthin film that remains stable for hours under ambient conditions (36). This feature means that thin-film experiments may achieve both high acceleration rates and high yields. For instance, a Katritzky reaction on a thin film on paper showed 100% conversion after 10 min, while the corresponding bulk reaction showed a conversion of less than 1% (30). For Schiff base derivatization of sugars in single-cell analysis, reaction in a thin film after 20 min showed 67% to 96% conversion ratios versus no conversion under bulk conditions (36). If one uses these data to calculate an apparent acceleration factor, the value is as high as 10^{11}. Obviously, such a number is unrealistic, as strong concentration effects due to solvent evaporation contribute to acceleration. To disentangle the concentration effect, investigators compared thin-film Schiff base reactions between primary amines and sugars in the neat (79) and paste-reaction formats (80), and in both cases control reactions were performed at the highest possible concentration. The intrinsic acceleration factor after correction for concentration was ~25 (36).

3. SCOPE OF CHEMISTRY

Table 1 summarizes the classes of reactions that have been successfully accelerated using different microdroplet-reaction methodologies, with examples of addition and elimination reactions as well as redox reactions. Besides organic synthetic reactions, including metal-catalyzed processes, both hydrogen–deuterium exchange and protein folding and unfolding were also found to be accelerated.

4. STUDY OF MECHANISMS

4.1. Enthalpy Effects: Partial Solvation of Reactants

Rate constants in the condensed phase are often dominated by ion pairing and solvent interactions, which mask the intrinsic reactivity of the reaction partners (5). The rate constants for substitution, addition and elimination, and redox and cycloaddition ion/molecule reactions in the gas phase are 10^{-12}–10^{-9} cm^3 $molecule^{-1}$ s^{-1}, corresponding to 10^8–10^{11} L mol^{-1} s^{-1} (2–10). However, the rate constants determined in solution phase are much smaller, varying from 10^0 to 10^5 L mol^{-1} s^{-1} (11, 89). Typically, there is a difference of six orders of magnitude between rate constants in gas-phase and solution-phase reactions (12, 89). In the condensed phase, desolvation represents a larger energy barrier to the reaction partners forming the transition state, an example of the solvent barrier effect (**Figure 2**). This effect alone will cause a 2–20 kcal mol^{-1} difference in activation energy between gas- and solution-phase reactions, which agrees roughly with the approximately six orders of magnitude difference in rate constants (89).

Partially solvated ions are the bridge between gas-phase and solution-phase reactions. For example, in the dilute gas phase of MS, various partially solvated ions, e.g., hydroxide, acylium, halide, alkali metal, and transition metal, have been generated and their reactivity investigated. In general, the ion/molecule reactivity of partially solvated ions decreases with increased cluster size (90). The degree of solvation also affects different reactions to different extents. In the S_N2 substitution reaction between solvated hydroxide anion and methyl halide, the reactivity of the monohydrated anion decreases to 60% and the dihydrated anion decreases to just 0.2% (90–92). This is a case in which partially solvated ions show quite different reactivity compared to unsolvated ions in gas-phase ion/molecule reactions. However, in sharp contrast, the extent of reaction between solvated hydroxide anion and carbon dioxide only decreases by 30% even with

Table 1 Reaction classes, general reaction schemes, and corresponding acceleration methods

Classification	Reactions	Chemical equations	Methods (reference)
1. Addition	1.1. Michael or aza-Michael addition	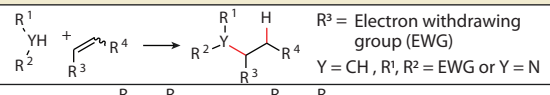	Reactive DESI (27) Dropcast thin film (29)
2. Elimination	2.1. Dehydration	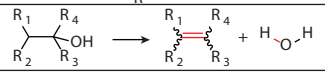	Leidenfrost droplet (50)
3. Addition and elimination	3.1. Schiff base formation	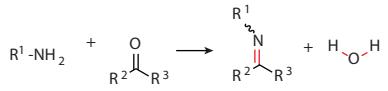	ESI (40) Reactive DESI (27) Dropcast thin film (36) Leidenfrost droplet (48)
	3.2. Claisen-Schmidt condensation	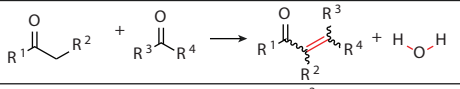	Preparative ESI (28) Leidenfrost droplet (48) Thin film (31, 33, 34)
	3.3. Katritzky transamination reaction	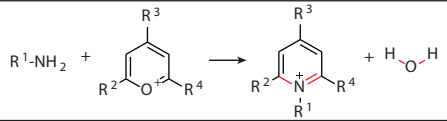	Leidenfrost droplet (50) Thin film (30, 34)
	3.4. Amide formation	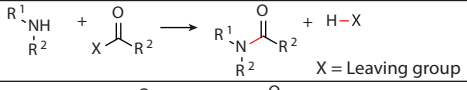	nESI (81) ESI (82)
	3.5. Hydrolysis of esters	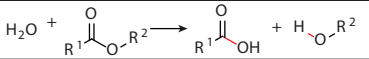	ESI (72)
4. Oxidation and reduction	4.1. Oxidation of amine or sulfide	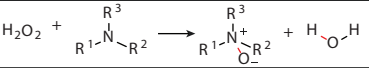	Levitated droplet (50)
	4.2. Synthesis of nanoparticles	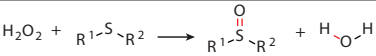	Levitated droplet (83) ESI (84)
5. Multi-component reaction	5.1. Mannich condensation	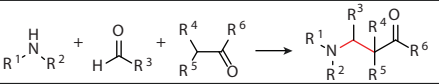	Thin film (30, 34)
	5.2. Hantzsch reaction	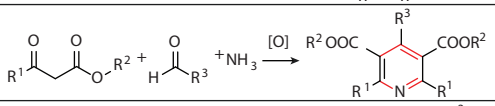	ESI (37)
	5.3. Biginelli reaction	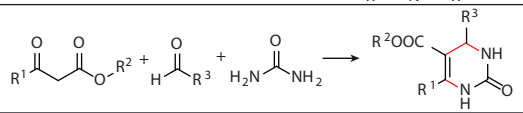	nESI (85)
6. Others	6.1. Hydrogen–deuterium exchange	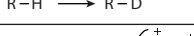	Droplet fusion (46) nESI (86)
	6.2. Protein folding and unfolding	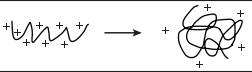	nESI (87) Droplet fusion (46)
	6.3. Organometallic reactions	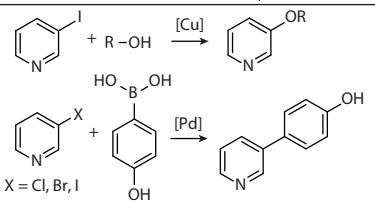	ESI and thin film (35) Levitated microdroplet (88)
	6.4. Pinacol rearrangement	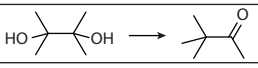	ESI (63)

Abbreviations: DESI, desorption electrospray ionization; ESI, electrospray ionization; nESI, nanoelectrospray ionization.

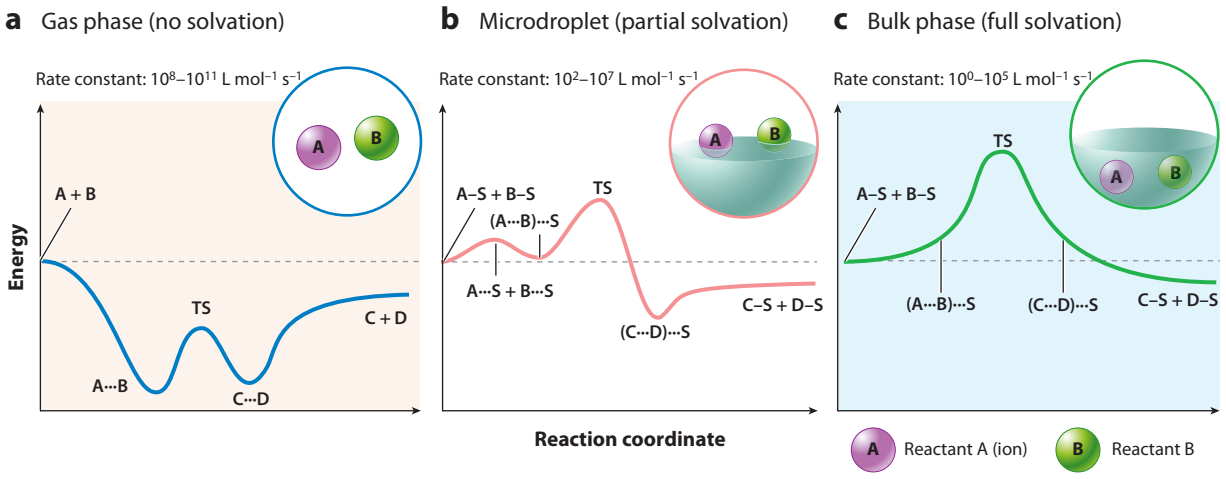

Figure 2

Schematic dependence of rate constants on reaction energy surfaces for the dilute gas phase, microdroplet interface, and bulk phase. A and B refer to two different reactants, S refers to solvent molecules, and C and D are two products. In order to make an analogy to gas-phase reactions, we assume A is the ionic form and B is neutral. A plus sign indicates that two particles are far from each other. An ellipsis indicates that the two particles are approaching but no bond is formed. A minus sign indicates bond formation. (*a*) Typical double-well energy surface for an ion/molecule reaction in vacuum. Reactants A and B approach each other, form A···B, overcome the activation energy to reach the transition state (TS), and form products C and D. (*b*) Energy surface for a microdroplet reaction. Partially solvated reactants A and B overcome the small solvation energy and approach each other, then overcome the activation energy to reach the TS, and form the products C and D. (*c*) Energy surface for the reaction in the bulk phase. Solvated reactants A and B overcome a large solvation energy as well as a large activation energy to reach the TS and form solvated products C and D.

20 molecules of hydration (with a hydration number of 0 to 20 and a rate constant of 2.5×10^{-9} to 1.7×10^{-9} cm^3 $molecule^{-1}$ s^{-1}) (90, 93–95). This is a case in which partially solvated ions show almost the same level of reactivity as the unsolvated gas-phase ions. As is well known to the MS community, partially solvated ions can be easily generated from coulombic explosions of charged microdroplets (1, 21). We propose that partial solvation of the reagents in microdroplets, like the partially solvated ions in ion/molecule reactions, will have intermediate-sized solvent barriers to reaction (see the sidebar titled Droplet Surface Reaction Versus Gas-Phase Ion/Molecule Reaction?). Looking at **Table 1**, we note the interesting fact that there is no confirmed report of

DROPLET SURFACE REACTION VERSUS GAS-PHASE ION/MOLECULE REACTION?

Because mass spectrometry is used as the detector in many microdroplet reaction studies, one might ask whether such chemistry is indeed droplet-surface chemistry rather than gas-phase ion chemistry. Overwhelming evidence exists for microdroplet reactions to be ascribed to the droplet interface. For example, (*a*) acceleration is observed for microdroplet reactions when methods other than mass spectrometry are used for product analysis. In these cases, droplets were collected and analyzed using HPLC-UV/vis or NMR analysis (or MS under conditions demonstrated not to cause reaction acceleration) (28, 51, 76). (*b*) Products of some reactions in the condensed phase are different from those of the corresponding ion/molecule reactions, but the microdroplet reactions produce products matching the condensed-phase products (41). (*c*) When intercepting droplets that partially evaporate as they travel, the same intermediates are seen as in the corresponding solution-phase reaction, the correspondence with reaction time would not be expected if the droplet reaction occurred in the dried droplets (37).

accelerated S_N2 substitution reactions, but many reports of accelerated reactions involving attack at carbonyl. This could be caused by the large reactivity difference in solvation of these two types of ions at the microdroplet surface.

4.2. Entropy Effects

Zare and coworkers (55) observed the ordered orientation of solute molecules in and near droplet surfaces using fluorescence polarization anisotropy. At the interface of water-in-oil microdroplets of rhodamine 6G, the rhodamine 6G dipole was observed to be oriented perpendicular to the interface. This ordered orientation must be due to electrostatic repulsion as a result of the increase in concentration density near the interface. The ordered orientation of the reactant molecules will decrease the entropy and increase the free energy of the initial state. For example, phosphorylation of ribose in bulk solution is thermodynamically unfavorable, at ΔG +5.4 kcal mol^{-1}. However, the same reaction displays ΔG −1.1 kcal mol^{-1} in microdroplets, where the entropic obstacle has been overcome by alignment of the reactant molecules in the microdroplet environment (45, 96). Another example, which, however, does not refer to solution–gas interfaces, is given by Baret and coworkers (56). A fluorescent imine formation reaction solution was segmented into small compartments with volumes of 2.5 to 160 pL. Both the rate constant and the equilibrium constant were observed to be inversely related to the droplet size. In 2.5-pL droplets, the authors achieved the largest apparent rate and equilibrium constants; these were 45-fold and 29-fold higher than those for the bulk phase, corresponding to a −2.3 kcal mol^{-1} change in activation energy and a −2.0 kcal mol^{-1} change in Gibbs free energy, respectively (56).

Ordered orientation can also apply to the solvent. There are extensive theoretical and experimental studies showing that interfacial water exhibits a layered structure due to the restricted rotational freedom of water dipoles near the surface (97). Water is likely to form ice-like structures in both the gas–liquid and solid–liquid interfacial regions. This makes the water near the surface less polar than that in the bulk. Very recently, the dielectric constant of confined water has been measured. With the decrease of water-film thickness confined in nanochannels of 1 to 100 nm, the dielectric constant of water decreases from 80 (bulk water value) to 1.8 (98, 99). Note that these values are even lower than are those for some typical nonpolar solvents such as cyclohexane, dioxane, diethyl ester, and ethyl acetate, whose dielectric constants are in the range of 2 to 8. These results indicate the Janus-like feature (100) of water in small confined volumes, which may explain the accelerated water–oil phase reactions in which use of phase-transfer catalysts is unnecessary (51). For instance, the Stevens oxidation of 4-nitrobenzyl alcohol with NaClO in ethyl acetate and water to form the aldehyde was reported to achieve a yield of 75% in the microdroplet reaction format without the use of any phase-transfer catalyst.

4.3. Fast Solvent Evaporation

A very rough model of evaporation posits that the evaporation rate is proportional to the surface area of liquid; therefore, the relative volume change caused by evaporation should be proportional to the surface-to-volume ratio (101, 102). If not controlled, evaporation significantly increases reagent concentration, causing a concentration effect on the reaction rate. In terms of pursuing the objective of achieving both high reaction rate and yield, the concentration effect is to be welcomed because it promotes the reaction both kinetically and thermodynamically. Solvent evaporation, especially in thin-film reactions, can result in reactions taking place with supersaturated reagents; this too will favor reactions with both a high rate and high yield, as many organic reactions are reversible (36). Typical examples are the dropcast thin-film Katritzky reaction (30)

and the Schiff base derivatization reaction for saccharide analysis in single cells (36). Both reactions display nearly 100% yield under thin-film conditions, compared to virtually no conversion under the corresponding bulk conditions. Note that at short times the kinetics of a reversible reaction can be measured directly without considering the influence of the back reaction (kinetic control). However, with increasing time, the influence of the back reaction becomes stronger, so the net reaction rate gradually approaches zero as equilibrium is approached (thermodynamic control). Due to limitations in droplet lifetime, making equilibrium measurements using microdroplet methods can be difficult. Therefore, acceleration factors for thin-film reactions are also measured in the kinetic control region for comparison. The concentration effect is a complication when one wants to measure intrinsic rate constants. As a result, the reaction rates in thin films are usually compared to neat or paste reactions to try to disentangle the contributions of concentration on the acceleration factor (36). The same case also occurs in levitated microdroplet experiments; however, there one can keep the concentration constant by adding back solvent to compensate for evaporation.

Evaporation also causes directed mass transfer in microdroplets and thin films, for example, by the coffee-ring (103) and Marangoni (104–106) effects. In thin-film reactions, reagents are dragged to the edges because of the larger solvent evaporation rate in these areas, namely the coffee-ring effect. In microdroplets, flow is directed from regions with low surface tension to high surface tension; solvent evaporation can cause surface-tension gradients, which result in the Marangoni flow in microdroplets. The Marangoni effect, also known as tears of wine, causes significant mass transfer in mixed-solvent systems with large differences in surface tension, such as the water–alcohol solvent system, in which alcohols display a lower surface tension and higher volatility. Faster evaporation of alcohol increases surface tension on the droplet surface and causes the Marangoni flow. This surface-tension-driven flow carries the reagents inward toward the droplet surface. These directed-mass-transfer effects in microdroplets (107) and thin films (108, 109) increase reaction rates by changing reagent distributions within the confined volume. One example of these effects providing significant acceleration is found for the Biginelli reaction in aqueous mixtures of methanol or ethanol—microdroplets of these solvents show more efficient product formation compared with pure methanol, ethanol, or water (85).

4.4. Fast Diffusion and Mixing

The partial-solvation hypothesis provides a good reason why reactions in the surface region are accelerated and achieve very high rate constants, while reactions in the droplet interior experience bulklike conditions. The surface region is a small fraction of the whole microdroplet; however, the overall acceleration of droplet reactions can be much greater than that accounted for by the contribution from the surface fraction. In fact, the fraction of the total number of reagents undergoing the fast surface reaction can be very large, if it is leveraged by efficient diffusion in the microdroplets. If the reaction rate in the surface region is much faster than that in the interior, reactants reach the surface, react, and diffuse back into the droplet bulk. The concentration gradient drives the diffusive flow until equilibrium is reached (**Figure 3**). In 2014, Baret and coworkers (56) presented an interfacial reaction-diffusion model to describe the influence of diffusion on reactions in small confined volumes. This model considers the parallel reactions in both the surface region and the interior, and free diffusion between the two regions based on Fick's second law. In the surface region, reactant molecules bind to the surface in ordered orientations and form products. The products can leave the surface and redistribute throughout the whole droplet. The authors provided support for their hypothesis by measuring the fluorescent imine produced in microdroplets of 2.5 and 160 pL (both concentrations in 15 mM) in an oil medium. Product fluorescence

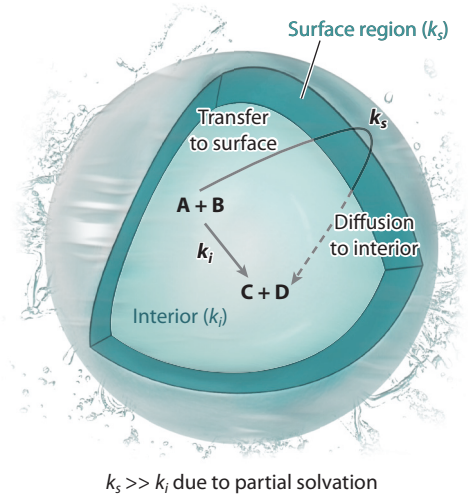

Figure 3

The influence of diffusion on the fraction of reagents undergoing fast surface reactions. The reaction rate in the surface region is much larger than that in the interior, so the diffusion rate influences the fraction of reactants undergoing reaction in the surface versus the interior region. A and B refer to two different reactants, and C and D are two products.

was observed only in the surface region of the 160-pL microdroplet, indicating fast reactions in the surface region. However, in the smaller 2.5-pL microdroplets, the fluorescent imine was observed to be uniformly distributed in the microdroplets, presumably because diffusion is more effective.

Microdroplets generated under ambient conditions experience turbulence caused by forces due to gas motion, liquid jets, and solvent evaporation that increase diffusion and mixing (52, 71). Mortensen & Williams (52) suggested that very fast mixing occurs in droplets generated by nanoelectrospray from a theta tip, an emitter with two separate channels carrying different solutions. In their estimate, the complete mixing time of two reagents in a theta tip was about 700 μs. However, they pointed out that the influence of turbulence could increase the mixing rate by three orders of magnitude according to ballistic microdroplet experiments, which is exactly the situation in Taylor cone jets observed in ESI. In the Leidenfrost-levitated droplets, so-called Leidenfrost wheels are observed that also increase mass-transfer efficiency in Leidenfrost reaction experiments (110). In a gravity-flattened Leidenfrost droplet, multiple Leidenfrost wheels can be formed in an individual droplet, forcing diffusion from the interior to the surface and back to the interior. In summary, the larger the diffusion coefficient is and the smaller is the droplet size, the larger is the measured reaction acceleration and the less anisotropy is in the microdroplet.

4.5. Summary of Mechanism of Accelerated Reactions in Microdroplets

Many factors cause the accelerated reactions in microdroplets, such as temperature, concentration, pressure, reagent orientation, and an increase in the intrinsic rate constant. The partial-solvation theory can explain the increase of intrinsic rate constants in the surface region of microdroplets. However, the overall acceleration of droplet reactions also often involves more than the contribution from the surface fraction of the reagents, indicating that the fraction of the total reagents

undergoing the fast surface reaction can be very large, provided that the reactant and product diffuse efficiently back and forth between the surface and interior of the microdroplets. Due to both the larger surface-to-volume ratio and the more effective diffusion within small volumes, reaction acceleration in microdroplets is much greater than that in larger droplets or in bulk. Besides these factors, the special interface physical and electrochemical properties such as extreme pH (111–114), abnormal dielectric constant (97–99), and surface potential (115) also contribute to making microdroplet chemistry different from bulk chemistry, and they need to be investigated more in the future.

5. APPLICATIONS

Reactions in confined volumes provide a new means to perform chemical synthesis, materials science, and analytical and biological chemistry (**Figure 4**).

5.1. Applications in Synthetic Chemistry

Reactions in confined volumes can occur at high reaction rates and produce products in high yields. The remaining question is how to perform accelerated synthesis at desirable scales. Promising systems for scaled-up synthesis likely require continuous reagent introduction, with recycling based on microdroplet or thin-film reaction. Such systems include Leidenfrost droplets (50), continuous deposition on substrate (28, 34, 51, 85), rotary evaporation (117), and multiplexed preparative paper sprays (118). In preparative electro- and pneumatic sprays, the continuous deposition of microdroplets of the reaction mixture on fiber, cotton, paper, or metal substrates allows the collection of reaction products at an approximately 1–100 mg h^{-1} scale. The scale of microdroplet synthesis can be further increased by simply multiplexing the sprayers. In preparative paper spray, such multiplexing has been achieved by using paper with 24 tips for scaled-up synthesis (118). In another simple scaled-up example, shrinking Leidenfrost droplets were used: Droplets containing large amounts of reagents can be shrunk from milliliters to microliters in minutes and then easily collected by siphoning the droplet from the well plate. In such a study, forced degradation of tetracycline produced a product with 99% purity (50). However, the large amount of solvent used in these experiments is environmentally undesirable (119). An ideal solution would be the development of a new generation of microdroplet reactors in which solvent is recycled for respraying in the system. Work toward such goals is under way.

5.2. Applications in Materials Science

Electrospray can be considered a component of an electrolytic cell in which reagents undergo redox reactions (120, 121). If one electrosprays positively charged microdroplets of metal ions, such as those of copper, silver, and gold, the formation of reduced metal particulates can be observed at the counter electrode (84). This provides an effective way to fabricate nanostructures on the collector surface (122). For example, nanoelectrospray of solutions of gold and silver salts yields nanoparticles of gold and silver at the collection surface, with an average size of 2.2 nm and 6.5 nm, respectively (84). These nanoparticles show high catalytic reactivity in the reduction of 4-nitrophenol by $NaBH_4$ in aqueous solution, with rate constants two orders of magnitude higher than those for nanoparticles synthesized by more conventional redox methods. By electrospraying metal ions through a partially masked plate, one can generate two-dimensional (2D)-patterned nanoparticle structures (116). For example, positive electrospray of a silver salt solution passing through a mask with an array of 200-μm holes generates an array of 20-μm

silver nanoparticles on the deposition plate. The pattern of the deposited nanoparticles matches that of the mask, but the sizes of the nanoparticle features are 10 times smaller than the mask hole sizes, a useful focusing effect of single apertures. Microdroplet reactions can also be used to fabricate nanowires. In the silver deposition experiment, metallic nanobrushes were observed on the mask surface as black circular spots around each mesh element. The speed of growth of the nanoparticles can be controlled by changing the metal salt concentration and the flow rate of

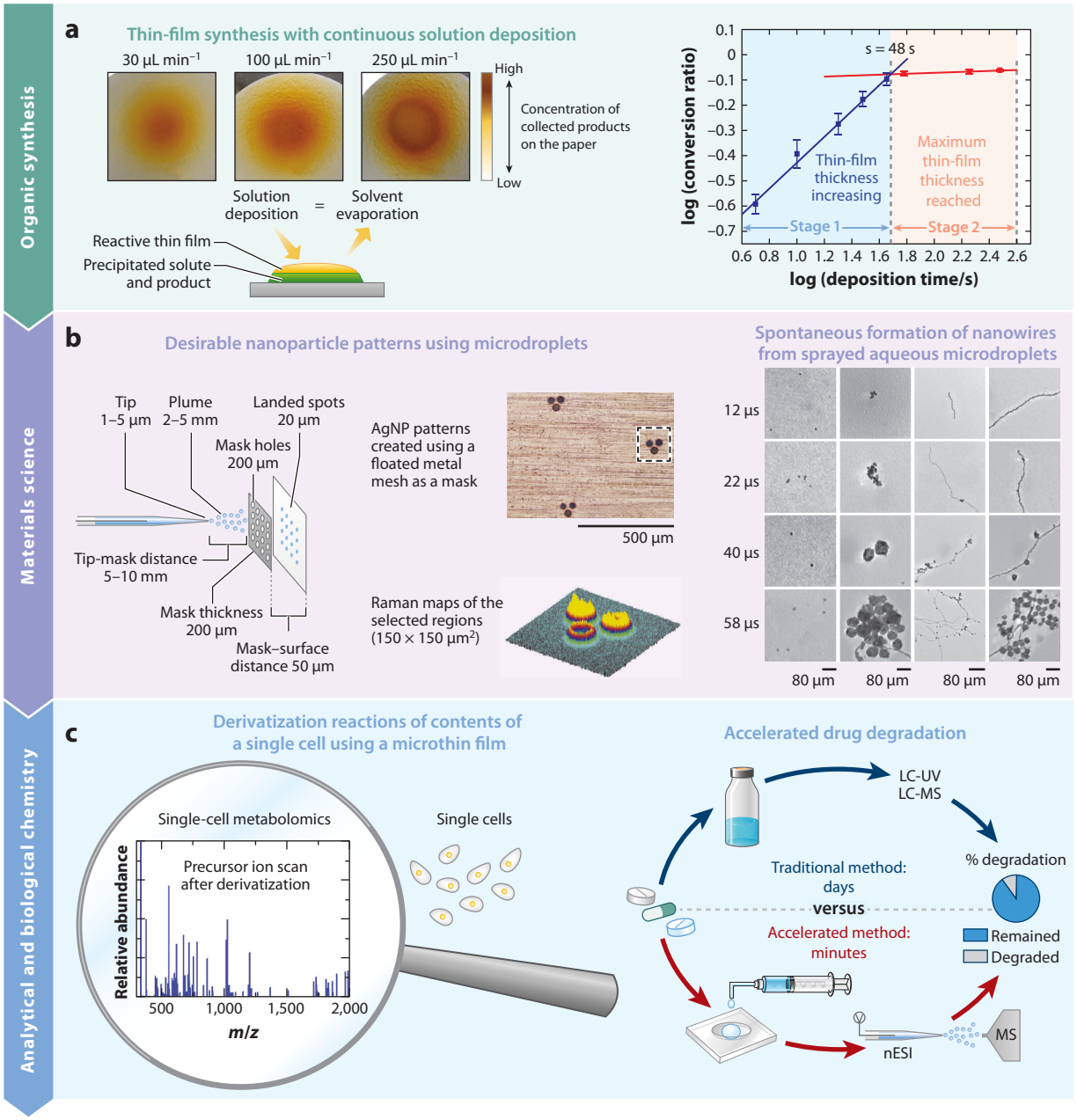

(*Caption appears on following page*)

Figure 4 (*Figure appears on preceding page*)

Typical applications of accelerated microdroplet reactions. (*a*) Applications in organic synthesis. (*Bottom left*) A schematic diagram of microdroplet synthesis and product collection on a paper substrate under ambient conditions. (*Top left*) The photos show the collected products in experiments using different reactant solution flow rates. (*Right*) The graph shows the reaction kinetics during thin-film growth before and after reaching dynamic equilibrium. Panel *a* adapted from Reference 34. (*b*) Applications of microdroplet chemistry in materials science. (*Left*) The diagram shows the use of ambient ion beams to write nanostructured patterns for use in surface-enhanced Raman spectroscopy. With a mesh mask, one can generate the desired patterns of AgNPs. (*Right*) The diagram shows the spontaneous formation of gold nanowires from sprayed aqueous microdroplets. Panel *b* adapted from References 44 and 116. (*c*) Bioanalytical applications of accelerated microdroplet reactions. (*Left*) The diagram shows the use of microthin films to perform accelerated chemical labeling and derivatization for saccharide characterization and identification from a single cell. (*Right*) The diagram shows the use of droplet reactions to accelerate the forced degradation of active pharmaceutical ingredients to satisfy pharmaceutical industry regulations. Panel *c* adapted from References 36 and 50. Abbreviations: AgNP, silver nanoparticle; LC-MS, liquid chromatography–mass spectrometry; LC-UV, liquid chromatography–ultraviolet; MS, mass spectrometry; nESI, nanoelectrospray ionization.

the electrospray (122). The growth of 1D nanowires might be due to the high electric field that exists at the tips of nanowires. However, a recent study reported the synthesis of gold nanowires in uncharged aqueous microdroplet streams without adding reducing agent (44). This could be because the polarization electrical field near the microdroplet–air interface helps direct the growth of nanowires. For example, the surface potential of water has been reported to be −18 mV with a maximum interfacial electric field of 8.9×10^7 V m^{-1} (115). The high electric field at the interface can alter both interfacial reactivity and ion transport through the vapor–liquid interface.

5.3. Analytical and Biological Applications

Samples of biological interest may be as small as or smaller than a single cell. The analysis of such systems has proven to be a challenge. The identification of trace components from biological media can require derivatization under mild conditions for successful MS analysis. Recently, the derivatization of sugars in a single onion cell has been performed using microthin film reactions to achieve both high reaction rate and yield (36). Only 1 nL of intracellular extract was transferred to a 500-nL droplet containing the nonvolatile derivatization reagent. After the fast evaporation of water under ambient conditions, a thin-film reactor was formed at a scale of several hundred picoliters, allowing for hours of stable reaction. The derivatization reaction is imine formation between the reducing sugars and *N*,*N*-dibutyl-1,3-propanediamine; the derivatization efficiency is 65–95%. To our knowledge, this is the only method that can perform effective derivatization in such small volumes.

Forced degradation studies have long been part of the development of active pharmaceutical ingredients. The acceleration of the degradation of pharmaceutical compounds has been exploited by the use of Leidenfrost conditions. Leidenfrost droplets yielded acceleration rates ranging from 23 to 188 when compared to the bulk degradation reactions, which means the typical forced degradation test time can be reduced from several days to a few hours. This rapid degradation method has the potential to be extended to the forced degradation of other pharmaceuticals and to drug formulations (50).

The microdroplet reactions also attract interest because the mechanisms leading to reaction acceleration in microdroplets can give insight into reactions in biological cells (61). In the microdroplet, gradients in reactant concentrations can form due to evaporation and directed mass transfer. This also applies to the diffusion of cellular constituents. Microdroplets represent a more-controlled and less-complex analog for cellular compartments, and they might be useful in modeling intracellular biological reactions.

DISCLOSURE STATEMENT

The authors are not aware of any affiliations, memberships, funding, or financial holdings that might be perceived as affecting the objectivity of this review.

ACKNOWLEDGMENTS

The authors thank Professor Hao Chen for valuable discussions. We acknowledge support from the Defense Advanced Research Projects Agency (DARPA) (grant W911NF-16-2-0020), the National Science Foundation (NSF) (grant 1905087), Merck & Co. (grant LKR174368), and Texas A&M University start-up funding to X.Y.

LITERATURE CITED

1. de Hoffmann E, Stroobant V. 2007. *Mass Spectrometry: Principles and Applications*. Hoboken, NJ: Wiley. 3rd ed.
2. Olmstead WN, Brauman JI. 1977. Gas-phase nucleophilic displacement reactions. *J. Am. Chem. Soc.* 99:4219–28
3. Freriks IL, De Koning LJ, Nibbering NMM. 1991. Gas-phase ambident reactivity of acyclic enolate anions. *J. Am. Chem. Soc.* 113:9119–24
4. Eberlin MN, Cooks RG. 1993. Polar [4+2+] Diels-Alder cycloadditions of acylium ions in the gas phase. *J. Am. Chem. Soc.* 115:9226–33
5. Gronert S. 2001. Mass spectrometric studies of organic ion/molecule reactions. *Chem. Rev.* 101:329–60
6. Pellerite MJ, Brauman JI. 1980. Intrinsic barriers in nucleophilic displacements. *J. Am. Chem. Soc.* 102:5993–99
7. Pellerite MJ, Brauman JI. 1983. Intrinsic barriers in nucleophilic displacements. A general model for intrinsic nucleophilicity toward methyl centers. *J. Am. Chem. Soc.* 105:2672–80
8. Dodd JA, Brauman JI. 1986. Marcus theory applied to reactions with double-minimum potential surfaces. *J. Phys. Chem.* 90:3559–62
9. Wladkowski BD, Wilbur JL, Brauman JI. 1994. Intrinsic structure-reactivity relationships in gas-phase S_N2 reactions: identity exchange of substituted benzyl chlorides with chloride ion. *J. Am. Chem. Soc.* 116:2471–80
10. Lum RC, Grabowski JJ. 1993. Carbon versus phosphorus site selectivity in the gas-phase anion molecule reactions of dimethyl methylphosphonate. *J. Am. Chem. Soc.* 115:7823–32
11. Denisov ET. 1974. *Liquid-Phase Reaction Rate Constants*. New York: Springer
12. Nelsen SF, Konradsson A, Jentzsch TL, O'Konek JJ, Pladziewicz JR. 2001. Comparison of gas and solution phase intrinsic rate constants for electron transfer of tetraalkylhydrazines. *J. Chem. Soc. Perkin Trans. 2* 9:1552–56
13. Page JS, Kelly RT, Tang K, Smith RD. 2007. Ionization and transmission efficiency in an electrospray ionization–mass spectrometry interface. *J. Am. Soc. Mass Spectrom.* 18:1582–90
14. Yergey AL, Yergey AK. 1997. Preparative scale mass spectrometry: a brief history of the calutron. *J. Am. Soc. Mass Spectrom.* 8:943–53
15. Siuzdak G, Bothner B, Yeager M, Brugidou C, Fauquet CM, et al. 1996. Mass spectrometry and viral analysis. *Chem. Biol.* 3:45–48
16. Badu-Tawiah AK, Wu C, Cooks RG. 2011. Ambient ion soft landing. *Anal. Chem.* 83:2648–54
17. Schwartz JC, Senko MW, Syka JEP. 2002. A two-dimensional quadrupole ion trap mass spectrometer. *J. Am. Soc. Mass Spectrom.* 13:659–69
18. Trauger SA, Junker T, Siuzdak G. 2003. Investigating viral proteins and intact viruses with mass spectrometry. In *Modern Mass Spectrometry*, ed. CA Schalley, pp. 265–82. Berlin/Heidelberg: Springer
19. Blake TA, Zheng OY, Wiseman JM, Takats Z, Guymon AJ, et al. 2004. Preparative linear ion trap mass spectrometer for separation and collection of purified proteins and peptides in arrays using ion soft landing. *Anal. Chem.* 76:6293–305

20. Gologan B, Green JR, Alvarez J, Laskin J, Cooks RG. 2005. Ion/surface reactions and ion soft-landing. *Phys. Chem. Chem. Phys.* 7:1490–500
21. Fenn JB, Mann M, Meng CK, Wong SF, Whitehouse CM. 1989. Electrospray ionization for mass spectrometry of large biomolecules. *Science* 246:64–71
22. Augusti R, Chen H, Eberlin LS, Nefliu M, Cooks RG. 2006. Atmospheric pressure Eberlin transacetalization reactions in the heterogeneous liquid/gas phase. *Int. J. Mass Spectrom.* 253:281–87
23. Cooks RG, Chen H, Eberlin MN, Zheng X, Tao WA. 2006. Polar acetalization and transacetalization in the gas phase: the Eberlin reaction. *Chem. Rev.* 106:188–211
24. Cotte-Rodriguez I, Chen H, Cooks RG. 2006. Rapid trace detection of triacetone triperoxide (TATP) by complexation reactions during desorption electrospray ionization. *Chem. Commun.* 2006:953–55
25. Chen H, Cotte-Rodriguez I, Cooks RG. 2006. *cis*-Diol functional group recognition by reactive desorption electrospray ionization (DESI). *Chem. Commun.* 2006:597–99
26. Wu C, Ifa DR, Manicke NE, Cooks RG. 2009. Rapid, direct analysis of cholesterol by charge labeling in reactive desorption electrospray ionization. *Anal. Chem.* 81:7618–24
27. Girod M, Moyano E, Campbell DI, Cooks RG. 2011. Accelerated bimolecular reactions in microdroplets studied by desorption electrospray ionization mass spectrometry. *Chem. Sci.* 2:501–10
28. Muller T, Badu-Tawiah A, Cooks RG. 2012. Accelerated carbon–carbon bond-forming reactions in preparative electrospray. *Angew. Chem. Int. Ed.* 51:11832–35
29. Badu-Tawiah AK, Campbell DI, Cooks RG. 2012. Accelerated C–N bond formation in dropcast thin films on ambient surfaces. *J. Am. Soc. Mass Spectrom.* 23:1461–68
30. Yan X, Augusti R, Li X, Cooks RG. 2013. Chemical reactivity assessment using reactive paper spray ionization mass spectrometry: the Katritzky reaction. *ChemPlusChem* 78:1142–98
31. Bain RM, Pulliam CJ, Yan X, Moore KF, Muller T, Cooks RG. 2014. Mass spectrometry in organic synthesis: Claisen-Schmidt base-catalyzed condensation and Hammett correlation of substituent effects. *J. Chem. Educ.* 91:1985–89
32. Bain RM, Pulliam CJ, Raab SA, Cooks G. 2016. Chemical synthesis accelerated by paper spray: the haloform reaction. *J. Chem. Educ.* 93:340–44
33. Li YF, Yan X, Cooks RG. 2016. The role of the interface in thin film and droplet accelerated reactions studied by competitive substituent effects. *Angew. Chem. Int. Ed.* 55:3433–37
34. Wei ZW, Wleklinski M, Ferreira C, Cooks RG. 2017. Reaction acceleration in thin films with continuous product deposition for organic synthesis. *Angew. Chem. Int. Ed.* 56:9386–90
35. Iyer K, Yi J, Bogdan A, Talaty N, Djuric SW, Cooks RG. 2018. Accelerated multi-reagent copper catalysed coupling reactions in micro droplets and thin films. *React. Chem. Eng.* 3:206–9
36. Wei ZW, Zhang XC, Wang JY, Zhang SC, Zhang XR, Cooks RG. 2018. High yield accelerated reactions in nonvolatile microthin films: chemical derivatization for analysis of single-cell intracellular fluid. *Chem. Sci.* 9:7779–86
37. Bain RM, Pulliam CJ, Cooks RG. 2015. Accelerated Hantzsch electrospray synthesis with temporal control of reaction intermediates. *Chem. Sci.* 6:397–401
38. Banerjee S, Zare RN. 2015. Syntheses of isoquinoline and substituted quinolines in charged microdroplets. *Angew. Chem. Int. Ed.* 54:14795–99
39. Lee JK, Banerjee S, Nam HG, Zare RN. 2015. Acceleration of reaction in charged microdroplets. *Q. Rev. Biophys.* 48:437–44
40. Bain RM, Pulliam CJ, Ayrton ST, Bain K, Cooks RG. 2016. Accelerated hydrazone formation in charged microdroplets. *Rapid Commun. Mass Spectrom.* 30:1875–78
41. Bain RM, Ayrton ST, Cooks RG. 2017. Fischer indole synthesis in the gas phase, the solution phase, and at the electrospray droplet interface. *J. Am. Soc. Mass Spectrom.* 28:1359–64
42. Chen XS, Cooks RG. 2018. Accelerated reactions in field desorption mass spectrometry. *J. Mass Spectrom.* 53:942–46
43. Lai YH, Sathyamoorthi S, Bain RM, Zare RN. 2018. Microdroplets accelerate ring opening of epoxides. *J. Am. Soc. Mass Spectrom.* 29:1036–43
44. Lee JK, Samanta D, Nam HG, Zare RN. 2018. Spontaneous formation of gold nanostructures in aqueous microdroplets. *Nat. Commun.* 9:1562

45. Nam I, Nam HG, Zare RN. 2018. Abiotic synthesis of purine and pyrimidine ribonucleosides in aqueous microdroplets. *PNAS* 115:36–40
46. Lee JK, Kim S, Nam HG, Zare RN. 2015. Microdroplet fusion mass spectrometry for fast reaction kinetics. *PNAS* 112:3898–903
47. Lee JK, Nam HG, Zare RN. 2017. Microdroplet fusion mass spectrometry: accelerated kinetics of acid-induced chlorophyll demetallation. *Q. Rev. Biophys.* 50:e2
48. Bain RM, Pulliam CJ, Thery F, Cooks RG. 2016. Accelerated chemical reactions and organic synthesis in Leidenfrost droplets. *Angew. Chem. Int. Ed.* 55:10478–82
49. Crawford EA, Esen C, Volmer DA. 2016. Real time monitoring of containerless microreactions in acoustically levitated droplets via ambient ionization mass spectrometry. *Anal. Chem.* 88:8396–403
50. Li YJ, Liu Y, Gao H, Helmy R, Wuelfing WP, et al. 2018. Accelerated forced degradation of pharmaceuticals in levitated microdroplet reactors. *Chem. Eur. J.* 24:7349–53
51. Yan X, Cheng HY, Zare RN. 2017. Two-phase reactions in microdroplets without the use of phase-transfer catalysts. *Angew. Chem. Int. Ed.* 56:3562–65
52. Mortensen DN, Williams ER. 2014. Theta-glass capillaries in electrospray ionization: rapid mixing and short droplet lifetimes. *Anal. Chem.* 86:9315–21
53. Ingram AJ, Boeser CL, Zare RN. 2016. Going beyond electrospray: mass spectrometric studies of chemical reactions in and on liquids. *Chem. Sci.* 7:39–55
54. Hollerbach A, Logsdon D, Iyer K, Li AY, Schaber JA, Cooks RG. 2018. Sizing sub-diffraction limit electrosprayed droplets by structured illumination microscopy. *Analyst* 143:232–40
55. Zhou ZP, Yan X, Lai YH, Zare RN. 2018. Fluorescence polarization anisotropy in microdroplets. *J. Phys. Chem. Lett.* 9:2928–32
56. Fallah-Araghi A, Meguellati K, Baret JC, El Harrak A, Mangeat T, et al. 2014. Enhanced chemical synthesis at soft interfaces: a universal reaction-adsorption mechanism in microcompartments. *Phys. Rev. Lett.* 112:028301
57. Houle FA, Wiegel AA, Wilson KR. 2018. Changes in reactivity as chemistry becomes confined to an interface. The case of free radical oxidation of $C_{30}H_{62}$ alkane by OH. *J. Phys. Chem. Lett.* 9:1053–57
58. Mondal S, Acharya S, Biswas R, Bagchi B, Zare RN. 2018. Enhancement of reaction rate in small-sized droplets: a combined analytical and simulation study. *J. Chem. Phys.* 148:244704
59. Yan X, Bain RM, Cooks RG. 2016. Organic reactions in microdroplets: reaction acceleration revealed by mass spectrometry. *Angew. Chem. Int. Ed.* 55:12960–72
60. Cooks RG, Yan X. 2018. Mass spectrometry for synthesis and analysis. *Annu. Rev. Anal. Chem.* 11:1–28
61. Stroberg W, Schnell S. 2018. Do cellular condensates accelerate biochemical reactions? Lessons from microdroplet chemistry. *Biophys. J.* 115:3–8
62. Dole M, Mack LL, Hines RL. 1968. Molecular beams of macroions. *J. Chem. Phys.* 49:2240–49
63. Chen H, Eberlin LS, Nefliu M, Augusti R, Cooks RG. 2008. Organic reactions of ionic intermediates promoted by atmospheric-pressure thermal activation. *Angew. Chem. Int. Ed.* 47:3422–25
64. Konermann L, Ahadi E, Rodriguez AD, Vahidi S. 2013. Unraveling the mechanism of electrospray ionization. *Anal. Chem.* 85:2–9
65. Kenny JA, Versluis K, Heck AJR, Walsgrove T, Wills M. 2000. The detection of intermediates in the ruthenium(II) catalysed asymmetric hydrogenation of ketones using electrospray ionisation mass spectrometry. *Chem. Commun.* 2000:99–100
66. Furmeier S, Metzger JO. 2004. Detection of transient radical cations in electron transfer-initiated Diels-Alder reactions by electrospray ionization mass spectrometry. *J. Am. Chem. Soc.* 126:14485–92
67. Marquez CA, Fabbretti F, Metzger JO. 2007. Electrospray ionization mass spectrometric study on the direct organocatalytic α-halogenation of aldehydes. *Angew. Chem. Int. Ed.* 46:6915–17
68. Yan X, Sokol E, Li X, Li GT, Xu SQ, Cooks RG. 2014. On-line reaction monitoring and mechanistic studies by mass spectrometry: Negishi cross-coupling, hydrogenolysis, and reductive amination. *Angew. Chem. Int. Ed.* 53:5931–35
69. Perry RH, Cahill TJ, Roizen JL, Du Bois J, Zare RN. 2012. Capturing fleeting intermediates in a catalytic C–H amination reaction cycle. *PNAS* 109:18295–99

70. Perry RH, Brownell KR, Chingin K, Cahill TJ, Waymouth RM, Zare RN. 2012. Transient Ru-methyl formate intermediates generated with bifunctional transfer hydrogenation catalysts. *PNAS* 109:2246–50
71. Mortensen DN, Williams ER. 2016. Ultrafast (1 μs) mixing and fast protein folding in nanodrops monitored by mass spectrometry. *J. Am. Chem. Soc.* 138:3453–60
72. Banerjee S, Gnanamani E, Yan X, Zare RN. 2017. Can all bulk-phase reactions be accelerated in microdroplets? *Analyst* 142:1399–402
73. Chen HW, Venter A, Cooks RG. 2006. Extractive electrospray ionization for direct analysis of undiluted urine, milk and other complex mixtures without sample preparation. *Chem. Commun.* 2006:2042–44
74. Davis RD, Jacobs MI, Houle FA, Wilson KR. 2017. Colliding-droplet microreactor: rapid on-demand inertial mixing and metal-catalyzed aqueous phase oxidation processes. *Anal. Chem.* 89:12494–501
75. Takats Z, Wiseman JM, Gologan B, Cooks RG. 2004. Mass spectrometry sampling under ambient conditions with desorption electrospray ionization. *Science* 306:471–73
76. Yan X, Lai YH, Zare RN. 2018. Preparative microdroplet synthesis of carboxylic acids from aerobic oxidation of aldehydes. *Chem. Sci.* 9:5207–11
77. Thomas DA, Wang LT, Goh B, Kim ES, Beauchamp JL. 2015. Mass spectrometric sampling of a liquid surface by nanoliter droplet generation from bursting bubbles and focused acoustic pulses: application to studies of interfacial chemistry. *Anal. Chem.* 87:3336–44
78. Jacobs MI, Davies JF, Lee L, Davis RD, Houle F, Wilson KR. 2017. Exploring chemistry in microcompartments using guided droplet collisions in a branched quadrupole trap coupled to a single droplet, paper spray mass spectrometer. *Anal. Chem.* 89:12511–19
79. Narayan S, Muldoon J, Finn MG, Fokin VV, Kolb HC, Sharpless KB. 2005. "On water": unique reactivity of organic compounds in aqueous suspension. *Angew. Chem. Int. Ed.* 44:3275–79
80. Gibard C, Bhowmik S, Karki M, Kim EK, Krishnamurthy R. 2018. Phosphorylation, oligomerization and self-assembly in water under potential prebiotic conditions. *Nat. Chem.* 10:212–17
81. Badu-Tawiah AK, Li AY, Jjunju FPM, Cooks RG. 2012. Peptide cross-linking at ambient surfaces by reactions of nanosprayed molecular cations. *Angew. Chem. Int. Ed.* 51:9417–21
82. Wleklinski M, Falcone CE, Loren BP, Jaman Z, Iyer K, et al. 2016. Can accelerated reactions in droplets guide chemistry at scale? *Eur. J. Org. Chem.* 2016:5480–84
83. Abdelaziz R, Disci-Zayed D, Hedayati MK, Pohls JH, Zillohu AU, et al. 2013. Green chemistry and nanofabrication in a levitated Leidenfrost drop. *Nat. Commun.* 4:2400
84. Li AY, Luo QJ, Park SJ, Cooks RG. 2014. Synthesis and catalytic reactions of nanoparticles formed by electrospray ionization of coinage metals. *Angew. Chem. Int. Ed.* 53:3147–50
85. Sahota N, AbuSalim DI, Wang ML, Brown CJ, Zhang ZCH, et al. 2019. A microdroplet-accelerated Biginelli reaction: mechanisms and separation of isomers using IMS-MS. *Chem. Sci.* 10:4822–27
86. Jansson ET, Lai YH, Santiago JG, Zare RN. 2017. Rapid hydrogen-deuterium exchange in liquid droplets. *J. Am. Chem. Soc.* 139:6851–54
87. Mortensen DN, Williams ER. 2015. Investigating protein folding and unfolding in electrospray nanodrops upon rapid mixing using theta-glass emitters. *Anal. Chem.* 87:1281–87
88. Fedick PW, Iyer K, Wei Z, Avramova L, Capek GO, Cooks RG. 2019. Screening of the Suzuki cross-coupling reaction using desorption electrospray ionization in high-throughput and in Leidenfrost droplet experiments. *J. Am. Soc. Mass Spectrom.* 30:2144–51
89. Caldwell G, Magnera TF, Kebarle P. 1984. SN2 reactions in the gas phase. Temperature dependence of the rate constants and energies of the transition states. Comparison with solution. *J. Am. Chem. Soc.* 106:959–66
90. Takashima K, Riveros JM. 1998. Gas-phase solvated negative ions. *Mass Spectrom. Rev.* 17:409–30
91. Viggiano AA, Arnold ST, Morris RA, Ahrens AF, Hierl PM. 1996. Temperature dependences of the rate constants and branching ratios for the reactions of $OH^-(H_2O)_{0–4} + CH_3Br$. *J. Phys. Chem.* 100:14397–402
92. Seeley JV, Morris RA, Viggiano AA. 1997. Temperature dependences of the rate constants and branching ratios for the reactions of $F^-(H_2O)_{0–5}$ with CH_3Br. *J. Phys. Chem. A* 101:4598–601

93. Yang X, Castleman AW. 1991. Chemistry of large hydrated anion clusters $X^-(H_2O)n$, $n = 0$–59 and X = OH, O, O_2, and O_3. 1. Reaction of CO_2 and possible application in understanding of enzymatic-reaction dynamics. *J. Am. Chem. Soc.* 113:6766–71
94. Yang X, Zhang X, Castleman AW. 1991. Chemistry of large hydrated anion clusters $X^-(H_2O)n$, $n = 0$–59 and X = OH, O, O_2, and O_3. 2. Reaction of Ch_3CN. *J. Phys. Chem.* 95:8520–24
95. Yang X, Castleman AW. 1991. Chemistry of large hydrated anion clusters $X^-(H_2O)n$, $n = 0$–59 and X = OH, O, O_2, and O_3. 3. Reaction of SO_2. *J. Phys. Chem.* 95:6182–86
96. Nam I, Lee JK, Nam HG, Zare RN. 2017. Abiotic production of sugar phosphates and uridine ribonucleoside in aqueous microdroplets. *PNAS* 114:12396–400
97. Toney MF, Howard JN, Richer J, Borges GL, Gordon JG, et al. 1994. Voltage-dependent ordering of water molecules at an electrode–electrolyte interface. *Nature* 368:444–46
98. Fumagalli L, Esfandiar A, Fabregas R, Hu S, Ares P, et al. 2018. Anomalously low dielectric constant of confined water. *Science* 360:1339–42
99. Kalinin SV. 2018. Feel the dielectric force. *Science* 360:1302
100. Nisisako T. 2016. Recent advances in microfluidic production of Janus droplets and particles. *Curr. Opin. Colloid Interface Sci.* 25:1–12
101. Chiu DT, Lorenz RM, Jeffries GDM. 2009. Droplets for ultrasmall-volume analysis. *Anal. Chem.* 81:5111–18
102. Chiu DT, Wilson CF, Ryttsen F, Stromberg A, Farre C, et al. 1999. Chemical transformations in individual ultrasmall biomimetic containers. *Science* 283:1892–95
103. Han W, Lin ZQ. 2012. Learning from "coffee rings": ordered structures enabled by controlled evaporative self-assembly. *Angew. Chem. Int. Ed.* 51:1534–46
104. Scriven LE, Sternling CV. 1960. The Marangoni effects. *Nature* 187:186–88
105. Sternling CV, Scriven LE. 1959. Interfacial turbulence: hydrodynamic instability and the Marangoni effect. *AIChE J.* 5:514–23
106. Mackay GDM, Mason SG. 1961. The Marangoni effect and liquid/liquid coalescence. *Nature* 191:488
107. Durey G, Kwon H, Magdelaine Q, Casiulis M, Mazet J, et al. 2018. Marangoni bursting: evaporation-induced emulsification of a two-component droplet. *Phys. Rev. Fluids* 3:100501
108. Sultan E, Boudaoud A, Ben Amar M. 2005. Evaporation of a thin film: diffusion of the vapour and Marangoni instabilities. *J. Fluid Mech.* 543:183–202
109. Fanton X, Cazabat AM, Quere D. 1996. Thickness and shape of films driven by a Marangoni flow. *Langmuir* 12:5875–80
110. Bouillant A, Mouterde T, Bourrianne P, Lagarde A, Clanet C, Quere D. 2018. Leidenfrost wheels. *Nat. Phys.* 14:1188–92
111. Banerjee S, Mazumdar S. 2012. Electrospray ionization mass spectrometry: a technique to access the information beyond the molecular weight of the analyte. *Int. J. Anal. Chem.* 2012:282574
112. Gatlin CL, Turecek F. 1994. Acidity determination in droplets formed by electrospraying methanol-water solutions. *Anal. Chem.* 66:712–18
113. Fenn JB. 1993. Ion formation from charged droplets: roles of geometry, energy, and time. *J. Am. Soc. Mass Spectrom.* 4:524–35
114. Gray-Weale A, Beattie JK. 2009. An explanation for the charge on water's surface. *Phys. Chem. Chem. Phys.* 11:10994–1005
115. Kathmann SM, Kuo IFW, Mundy CJ. 2008. Electronic effects on the surface potential at the vapor-liquid interface of water. *J. Am. Chem. Soc.* 130:16556–61
116. Li AY, Baird Z, Bag S, Sarkar D, Prabhath A, et al. 2014. Using ambient ion beams to write nanostructured patterns for surface enhanced Raman spectroscopy. *Angew. Chem. Int. Ed.* 53:12528–31
117. Schrader RL, Fedick PW, Mehari TF, Cooks RG. 2019. Accelerated chemical synthesis: three ways of performing the Katritzky transamination reaction. *J. Chem. Educ.* 96:360–65
118. Zhu XT, Zhang WW, Lin QY, Ye MY, Xue LY, et al. 2019. Direct microdroplet synthesis of carboxylic acids from alcohols by preparative paper spray ionization without phase transfer catalysts. *ACS Sustain. Chem. Eng.* 7:6486–91
119. Sheldon RA. 2007. The E factor: fifteen years on. *Green Chem.* 9:1273–83

120. Van Berkel GJ, Zhou FM. 1995. Electrospray as a controlled-current electrolytic cell: electrochemical ionization of neutral analytes for detection by electrospray mass spectrometry. *Anal. Chem.* 67:3958–64
121. Van Berkel GJ, Zhou FM. 1995. Characterization of an electrospray ion-source as a controlled-current electrolytic cell. *Anal. Chem.* 67:2916–23
122. Sarkar D, Mahitha MK, Som A, Li AY, Wleklinski M, et al. 2016. Metallic nanobrushes made using ambient droplet sprays. *Adv. Mater.* 28:2223–28

Annual Review of
Physical Chemistry
Volume 71, 2020

Contents

Errata

An online log of corrections to *Annual Review of Physical Chemistry* articles may be found at http://www.annualreviews.org/errata/physchem